Available online at www.sciencedirect.com
ScienceDirect
Surface Science 601 (2007) 5394–5402
SURFACE SCIENCE
www.elsevier.com/locate/susc

Identification of the vanadyl terminated $V_2O_3(0001)$ surface by NEXAFS spectroscopy: A combined theoretical and experimental study

C. Kolczewski [a], K. Hermann [a,*], S. Guimond [b], H. Kuhlenbeck [b], H.-J. Freund [b]

[a] *Theory Department, Fritz-Haber-Institut der Max-Planck-Gesellschaft, Faradayweg 4-6, D-14195 Berlin, Germany*[1]
[b] *Chemical Physics Department, Fritz-Haber-Institut der Max-Planck-Gesellschaft, Faradayweg 4-6, D-14195 Berlin, Germany*[1]

Received 5 June 2007; accepted for publication 3 September 2007
Available online 12 October 2007

Abstract

In this work we present results from density functional theory (DFT) cluster studies to determine polarization-dependent near edge X-ray absorption fine structure (NEXAFS) spectra of the vanadyl termination of the $V_2O_3(0001)$ surface. The oxygen K edge spectra are calculated for the relaxed surface geometry where geometric parameters are taken from recent periodic DFT work. A detailed analysis of energetic peak positions, relative intensities, and final state orbitals allows a deep understanding of the complex angular dependence of the calculated spectra on the basis of the local binding environment of differently coordinated oxygen species. Further, our theoretical analysis can assign and explain various spectral details in the experimental NEXAFS data, in particular, those related to vanadyl oxygen. This allows us to support the experimentally suggested vanadyl surface termination.

Keywords: Density functional calculations; Near edge extended X-ray absorption fine structure (NEXAFS); Vanadium oxides

1. Introduction

Vanadium sesquioxide, V_2O_3, is a member of a large vanadium oxide family where the oxidation number of vanadium ranges from +5 in V_2O_5 to +2 in VO [1]. This causes a variety of interesting structural and electronic properties, making vanadium oxides interesting both for scientific research and industrial applications. Vanadium oxide based catalysts are used for a number of different chemical reactions [2–7] such as oxidation of SO_2 and hydrocarbons or the selective reduction of NO_x with ammonia. Here we focus on V_2O_3 since it is often argued that the catalytic activity of vanadium oxide based catalysts is due to the presence of vanadium species with a lower vanadium oxidation state (see [8] and references therein). V_2O_3 is produced as a product of deep reduction of vanadium pentoxide in many catalytic reactions. It undergoes a phase transition from an anti-ferromagnetic semiconductor with monoclinic crystal structure below 150–170 K to a paramagnetic metal with rhombohedral corundum structure above the transition temperature [9].

While the structure and the physical/chemical properties of bulk V_2O_3 have been studied extensively both by theory and experiment [10–13], only two types of V_2O_3 surfaces, of single crystal orientation (0001) and (10–12), have been examined in greater detail [14–17]. Here the (0001) surface seems to be more easily accessible by experiment [16]. Rhombohedral V_2O_3 bulk crystals are described along their (0001) direction by stacking alternating hexagonal netplanes of vanadium (two very close planes, V and V') and oxygen (one plane O) in the sequence ...OVV'OVV'... This allows three bulk truncated terminations denoted OVV', VV'O, and V'OV, see Fig. 1. In addition, several

* Corresponding author.
E-mail address: hermann@fhi-berlin.mpg.de (K. Hermann).
[1] Sonderforschungsberich Sfb 546 Transition Metal Oxide Aggregates, Berlin, Germany.

0039-6028/$ - see front matter © 2007 Elsevier B.V. All rights reserved.
doi:10.1016/j.susc.2007.09.033

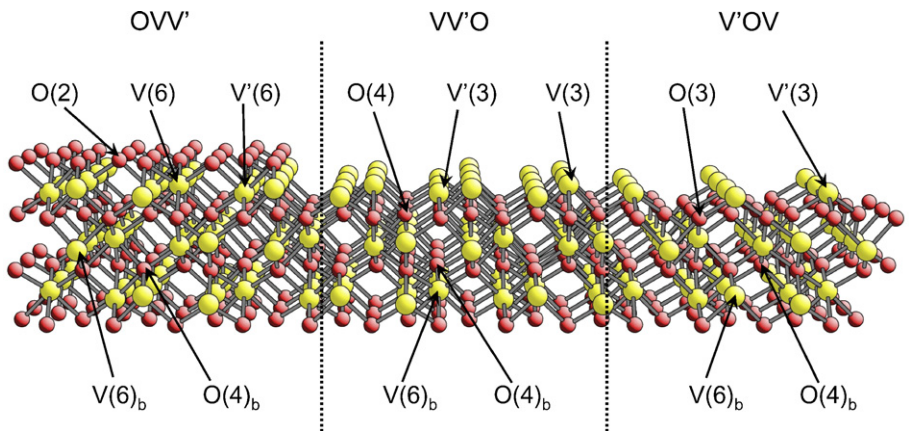

Fig. 1. Crystal structure of rhombohedral V_2O_3 with plane stacking along (0001) sketching the OVV', VV'O, and V'OV termination of the (0001) surface. The different netplanes are labeled accordingly (numbers in parenthesis denote the local coordination) where vanadium centers are shown by large (yellow) balls and oxygen centers by small (red) balls. Neighboring atom centers are connected by sticks to visualize structural details. (For interpretation of the references to color in this figure, the reader is referred to the web version of this article.)

experimental and theoretical studies have found that, depending on surface preparation, temperature, and pressure, other terminations can arise including substantial reconstruction where atoms of lower lying bulk layers move to the surface [14,15,18–26]. As an example we mention recent experimental work on thick $V_2O_3(0001)$ films on Rh(111) [20]. Reactive metal deposition at a substrate temperature of 250 °C and an oxygen pressure of 2×10^{-7} mbar followed by annealing in UHV to 600 °C yields atomically flat $V_2O_3(0001)$-(1×1) surfaces terminated by vanadyl (V=O) groups. Under more oxidizing conditions the vanadyl terminated surface transforms into an oxygen rich reconstructed $V_2O_3(0001)$-$(\sqrt{3}\times\sqrt{3})R30°$ surface removing up to one half of the vanadyl groups, while the deposition of submonolayer vanadium coverages onto the $V_2O_3(0001)$-(1×1) surface results in atomically flat terraces terminated by a metastable close-packed V_3 layer on top of the O layer (see Ref. [20] for further details). Theoretical studies of the surface structure and energetics of $V_2O_3(0001)$ as obtained by periodic density functional theory (DFT) [15] confirm the experimental results mentioned above. Here the surface either adopts a hexagonal tri-layer structure or a vanadyl terminated modification where the latter is the dominant and stable phase if the surface is in thermal equilibrium with the V_2O_3 bulk [15]. Further, recent theoretical work on thin V_2O_3 films supported on α-alumina combining DFT and statistical thermodynamics suggest that ultrathin films terminated by (1×1) vanadyl groups are stable at room temperature and ultrahigh vacuum (UHV) conditions [27].

These findings lead to the conclusion that the vanadyl terminated surface is the most stable when it is in thermal equilibrium with the V_2O_3 bulk whereas the ideal bulk terminations are less favorable [15]. The vanadyl terminated surface can be derived in the simplest case from the ideal half metal layer termination by covering each vanadium of the topmost layer with an additional oxygen atom forming a vanadyl group [26]. This surface termination will be denoted $O_tV'OV$ in the following (the nomenclature reflects the elemental composition of the top most layers). It is characterized by three kinds of differently coordinated oxygen: singly coordinated vanadyl oxygen at the top,

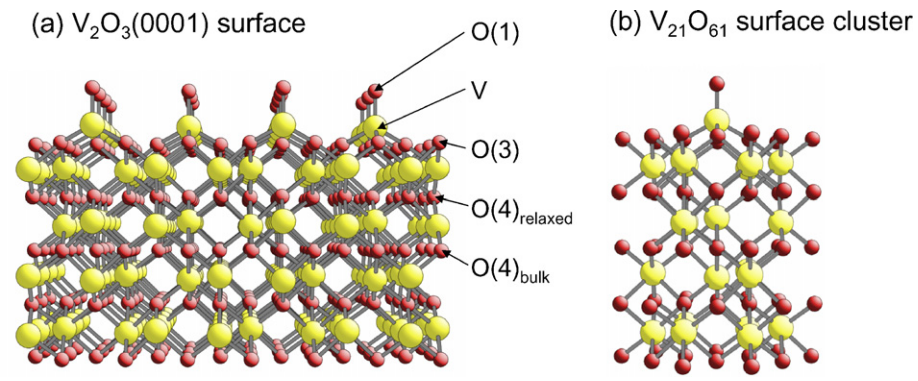

Fig. 2. (a) Crystal structure of the ideal vanadyl terminated $V_2O_3(0001)$ surface with differently coordinated oxygen species indicated. (b) Cluster model $V_{21}O_{61}$ for the vanadyl terminated surface. Vanadium centers are shown by large (yellow) balls and oxygen centers by small (red) balls. The cluster coordinates are taken from periodic slab calculations [15]. (For interpretation of the references to color in this figure, the reader is referred to the web version of this article.)

three fold coordinated oxygen in the first oxygen layer, and four fold coordinated bulk oxygen, see Fig. 2a. The different coordination is expected to lead to different chemical behavior of the oxygen species. Therefore, it is important to study their electronic properties as a function of local coordination. This may also help to interpret experimental data from various spectroscopic techniques, such as vibrational or near edge X-ray absorption fine structure (NEXAFS) spectroscopy, thus, allowing a discrimination of differently coordinated oxygen based on experimental information. The discrimination could be of interest in studies of catalytic reactions where adsorption sites of small molecules like water [28] or methanol [29–31] have to be identified.

In this work we use ab initio density functional theory (DFT) together with cluster models to evaluate the electronic structure of local environments at the $V_2O_3(0001)$ surface where we focus on the vanadyl terminated surface. The electronic structure then serves as a basis to calculate polarization-dependent NEXAFS spectra for 1s core excitations of oxygen centers near the $V_2O_3(0001)$ surface. The theoretical data are compared with experimental NEXAFS spectra of thin $V_2O_3(0001)$ films on W(110) and Au(111) which help to confirm the surface termination suggested by experiment. This paper extends earlier studies on this system [24,32].

In Sections 2 and 3 we describe computational and experimental details of the present work while in Section 4 we present results together with a detailed comparison of experimental and theoretical polarization-dependent NEXAFS spectra of the vanadyl terminated $V_2O_3(0001)$ surface. Finally, in Section 5 we summarize our results and conclusions.

2. Computational details

Below the phase transition temperature of $T_s = 150$–170 K, vanadium sesquioxide, V_2O_3, is described by a monoclinic (distorted corundum) crystal lattice with lattice constants $a = 7.26$ Å, $b = 5.00$ Å, $c = 5.55$ Å, and angle $\beta = 96.75°$ [33,34] where the unit cell contains 20 atoms (four V_2O_3 elemental units). Above T_s the oxide assumes a rhombohedral corundum structure where the corresponding lattice constants and angles are $a = b = c = 5.46$ Å and $\alpha = 53.75°$ [35,36] and the unit cell includes two elemental units, i.e. 10 atoms. Bulk crystals of both lattice structures contain vanadium in six fold octahedral and oxygen in four fold tetrahedral coordination. Apart from a doubling of the unit cell size in going from the rhombohedral to the monoclinic lattice there are only very small structural differences between the two V_2O_3 crystal lattices. Therefore, in the present study we focus on the rhombohedral corundum structure which is of higher symmetry compared with that of the monoclinic system.

A local section of the vanadyl terminated $O_tV'OV$ surface is modeled by a cluster of finite size where the coordinates of the atoms are taken from recent periodic slab calculations [15]. The cluster consists of 21 vanadium and 61 oxygen atoms, see Fig. 2b. No effort was made to saturate dangling bonds of peripheral oxygen (electronic embedding) [25] since the present work deals only with electronic properties of oxygen very close to the center of a fairly large cluster. Extensive test calculations with clusters of similar size have shown that the electronic structure near the inner cluster region is affected only very little by the presence of dangling bonds at the cluster periphery.

The electronic structure of the present cluster is calculated by ab initio density functional theory (DFT) methods (program code StoBe [37]) using generalized gradient corrected functionals according to Perdew, Burke, and Ernzerhof (RPBE) [38,39] to approximate electron exchange and correlation. The Kohn–Sham orbitals are described by linear combinations of atomic orbitals (LCAO's) using extended basis sets of contracted Gaussians from atom optimizations [40,41]. The molecular basis sets used in the ground state calculations are all-electron double zeta plus valence polarization (DZVP) type for vanadium and oxygen, described by [5s3p2d] and by [3s2p1d], respectively. The vanadium basis is also used in the calculations of O 1s core excitation while for oxygen different basis sets are applied. The basis set at the excited oxygen center is IGLO-III [42] characterized as [7s6p2d] in order to obtain an adequate description of inner shell relaxation effects. The other oxygen centers in the cluster are accounted for by effective core potentials (ECP) including their 1s electrons and [3s3p1d] valence basis sets [43] to avoid explicit mixing of 1s orbitals of different oxygen centers. This approximation is found to result in faster convergence of the electronic structure introducing only negligible effects on the computed excitation spectra [44].

The calculations of O 1s core level excitation spectra is performed within Slater's transition potential (TP) approach [45,46] in combination with a double basis set technique [47]. This approach starts from a self-consistent transition potential calculation with a partially occupied O 1s core orbital at the ionization site ($n_{O\,1s} = 0.5$ according to Slater [45,46]). The resulting orbital energies and corresponding dipole transition matrix elements (determining absorption intensities) are then used to compute the theoretical NEXAFS spectra by Gaussian convolution with varying broadening. A broadening of 0.5 eV is applied below ionization threshold while within 10 eV above threshold the broadening is increased linearly to 4.5 eV and kept fixed at this value for higher energies [48]. For further details see also Refs. [49–51].

In Slater's transition potential approach the electronic core hole relaxation of the excited final state is not fully accounted for. This incomplete relaxation can be corrected in an approximate way by shifting all excitation energies by the difference of the ionization potential evaluated with the TP method and the corresponding value from ΔKohn–Sham (ΔSCF) calculations, resulting in a global relaxation shift of 1.8–1.9 eV to lower energies. Further, all spectra are shifted by 0.4 eV to higher energies to in-

clude relativistic corrections [52] (in a recent work [53], the shift is revised to 0.33 eV). Altogether, this results in a global downwards shift of 1.4 eV which has to be applied when the present theoretical NEXAFS spectra are to be compared with experimental spectra.

The calculation of NEXAFS spectra in the present work is based on core to unoccupied orbital excitations which are determined by dipole transitions. Hence, polarization-resolved spectral intensities $I(E, \vartheta, \varphi)$ are given by corresponding dipole transition matrix elements $\{m\} = (m_x, m_y, m_z)$ together with angle dependent factors described by the polarization vector $e = (e_x, e_y, e_z)$ of the incoming radiation yielding

$$\begin{aligned} I(E,\vartheta,\varphi) &= \kappa \cdot E \cdot (\underline{m}\underline{e})^2 \\ &= \kappa \cdot E \cdot (m_x e_x + m_y e_y + m_z e_z)^2 \\ &= \kappa \cdot E \cdot \{\sin^2\vartheta (m_x \cos\varphi + m_y \sin\varphi)^2 \\ &\quad + \cos^2\vartheta m_z^2 + 2\sin\vartheta\cos\vartheta (m_x\cos\varphi + m_y \\ &\quad \times \sin\varphi) m_z\} \end{aligned} \tag{1}$$

where E denotes the transition energy and κ is a global scaling factor. The dipole transition matrix elements are vector quantities (dipole transition vectors) $m = (m_x, m_y, m_z)$ which involve the initial core orbital φ_i and final excited state orbital φ_f reading

$$\underline{m} = (m_x, m_y, m_z) = \langle \varphi_f \mid q \cdot \underline{r} \mid \varphi_i \rangle \tag{2}$$

and the polarization vector e is written as

$$\underline{e} = (e_x, e_y, e_z) = (\sin\vartheta\cos\varphi, \sin\vartheta\sin\varphi, \cos\vartheta) \tag{3}$$

For the hexagonal structure of the present $V_2O_3(0\,0\,0\,1)$ surface and the experimental photon beam geometry to be discussed in Section 3 the spectral intensities, Eq. (1), simplify to

$$I(E,\vartheta) = \kappa \cdot E \cdot \{1/2[m_x^2 + m_y^2]\sin^2\vartheta + m_z^2\cos^2\vartheta\} \tag{1a}$$

depending only on the polar angle ϑ of the photon polarization vector. This can be converted into

$$I(E,\alpha) = \kappa \cdot E \cdot \{1/2[m_x^2 + m_y^2]\cos^2\alpha + m_z^2\sin^2\alpha\} \tag{1b}$$

where α is the angle of the photon beam with respect to the surface normal. Eq. (1b) is used to calculate all theoretical angle-resolved NEXAFS spectra presented in this work.

3. Experimental details

NEXAFS spectra were recorded with light from the U56/2-PGM1 beam line at the BESSY II storage ring. A home-made partial yield detector (PYD) mounted at an angle of 70° with respect to the incoming photon beam was used for detection. The voltages required for the channeltron of the PYD were provided by a home-made battery box and a Keithley 6517A electrometer was employed to detect the incoming electron current amplified by the channeltron. To enhance the surface sensitivity the retarding grid in front of the detector was set to a voltage of −50 V which prevents electrons with energies smaller than 50 eV from reaching the channeltron. The beam line monochromator was set to deliver a photon flux with an energy spread of better than 70 meV.

The Au(1 1 1) substrate sample was mounted on a manipulator equipped with a sample holder providing rotation to change the azimuthal light incidence angle. The polar light incidence angle could be changed via rotation of the manipulator axis. Sample annealing was possible by heating the mounting plate of the sample holder with electrons emitted from a tungsten filament. For temperature control a NiCr/Ni thermocouple was inserted into a small hole drilled into the crystal side.

The Au(1 1 1) substrate was cleaned in UHV by cycles of argon sputtering and annealing at 1050 K. The $V_2O_3(0\,0\,0\,1)$ film was prepared by evaporation of metallic vanadium (using an Omicron EFM4 electron beam evaporator) in an oxygen atmosphere (10^{-7} mbar) at 600 K followed by annealing at 670 K in 10^{-7} mbar of oxygen and annealing in vacuum at 850 K. The evaporator was calibrated using a quartz microbalance. Evaporation rates between 0.5 and 1 Å/min were employed in the experiments. The prepared $V_2O_3(0\,0\,0\,1)$ films were usually about 100 Å thick and exhibited a well-defined hexagonal LEED pattern as expected for the (0 0 0 1) surface of a corundum type structure.

It has been shown earlier [54] that vanadyl terminated $V_2O_3(0\,0\,0\,1)$ films do not accumulate OH groups at their surfaces. However, the vanadium terminated $V_2O_3(0\,0\,0\,1)$ film surface is sensitive to surface hydroxilation via decomposition of water [54]. To avoid extensive hydroxyl contamination the vanadium terminated surface was reoxidized frequently to establish the vanadyl terminated surface followed by reduction via electron irradiation to reproduce the vanadium terminated surface. This procedure is known to remove hydroxyl groups from the surface since in involves annealing at temperatures where the hydroxyl groups vanish from the surface [54].

4. Results and discussion

Theoretical polarization-dependent NEXAFS spectra of singly coordinated vanadyl oxygen O(1) at the $O_tV'OV$ terminated $V_2O_3(0\,0\,0\,1)$ surface are shown in Fig. 3a. The spectra can be divided roughly into two energy regions, a region below ionization threshold (the corresponding ionization potential (IP) amounts to 539.4 eV) and one above. The latter is assigned to O 1s → O 3p transitions which will not be discussed in the present context. In our analysis we focus on the low energy part which shows a rather complex peak structure between 530 eV and 533 eV. These peaks can be assigned to transitions into final state orbitals which are anti-bonding combinations of O 2p and V 3d orbitals. The energetic positions of the participating excitations are determined by the anti-bonding character of the corresponding final state orbital: the stronger the anti-bonding

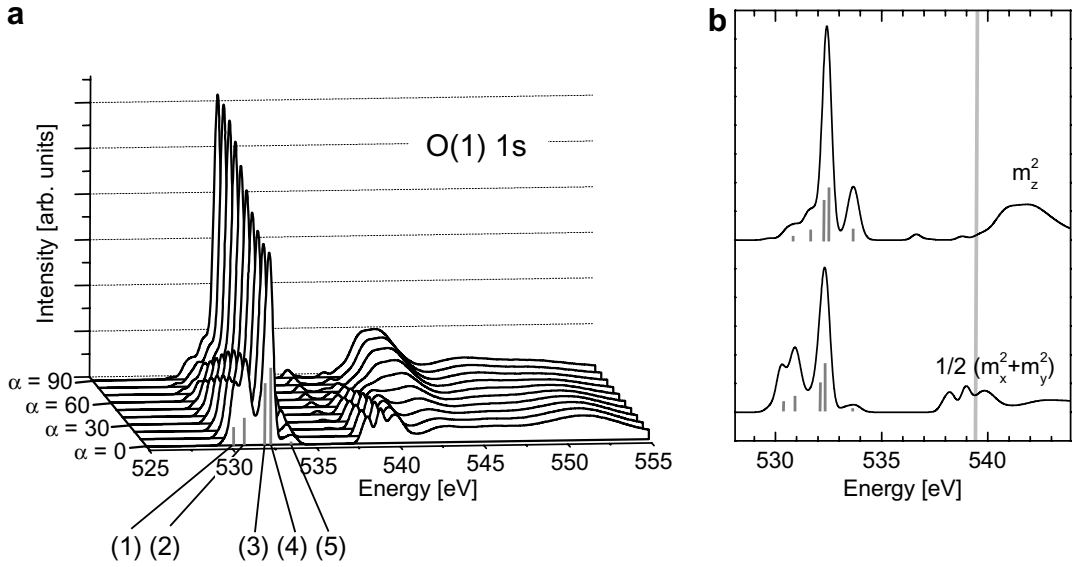

Fig. 3. Theoretical polarization-dependent NEXAFS spectra for the vanadyl terminated $V_2O_3(0001)$ surface: (a) Spectra of singly coordinated vanadyl oxygen, O(1), in the first surface layer. The angle of incidence of the photon beam α is given with respect to the surface normal. (b) Squared transition dipole matrix elements for O(1) 1s core excitations. The vertical gray line indicates the ionization threshold. Note that in both figures the energy scale has not been corrected for core hole relaxation and relativistic effects, see Section 2.

characters of the final state orbital, the higher the energy of the corresponding transition.

The complex angle dependence in the polarization-dependent spectra can be understood by the directions of the corresponding dipole transition vectors m, see Eq. (2), determining the transition intensities. Since vector m involves the O 1s orbital as the initial state orbital only transitions into final state orbitals which have non-vanishing O p contributions (in the present work only O 2p in the low energy part of the spectrum) can appear in the spectrum. If the O p component of the final state orbital is oriented parallel to the surface, the dipole transition vector will point along the x- and/or y-direction (the coordinate system is oriented such that the x- and y-axes are parallel and the z-axis is normal to the surface). If the O p component is oriented perpendicular to the surface then the z-component of m will be large. Based on these results, the angular dependence of the O(1) 1s spectrum (Fig. 3a) can be analyzed in further detail. The final state orbitals corresponding to the most prominent O(1) 1s excitations (indicated by vertical lines in Fig. 3a) are given in Fig. 4, where the labeling of the molecular orbitals is in ascending energetic order according to the excitations in Fig. 3a. A close inspection of Fig. 4 shows that orbitals (1)–(3) are characterized near the oxygen center O(1) by O 2p contributions, p_x and p_y, parallel to the surface such that the corresponding dipole transition vector contains large m_x, m_y components. Therefore, the peaks referring to final state orbitals (1)–(3), are large for small photon incidence angles α and decrease with increasing α according to Eq. (1b). The final state orbital corresponding to peak (4) contains perpendicular $2p_z$ components near the oxygen center O(1). Consequently, the dipole transition vector has a large m_z component and the intensity of peak (4) is small for small photon incidence angles α and increasing with increasing α. Since transitions (3) and (4) belong to final state orbitals which are very close in energy, the two intensity contributions complement each other and only a weak angle dependence is found. Finally, peak (5) shows an increasing intensity with increasing α which is explained by the dipole transition vector involving orbital (5) of $2p_z$ character near the O(1) center as shown in Fig. 4.

The complex angle dependence can be illustrated further by plotting the squared transition dipole matrix elements parallel to the surface, $m_{\parallel} = 1/2(m_x^2 + m_y^2)$, and perpendicular to it, $m_{\perp} = m_z^2$, see Fig. 3b. For a photon angle $\alpha = 0°$ the corresponding NEXAFS spectrum is determined by quantity $m_{\parallel}$, see also Eq. (1b), whereas for $\alpha = 90°$ $m_{\perp}$ is decisive. For intermediate angles the NEXAFS spectrum consists of a superposition of both parts weighted by the corresponding angular factors. Thus, Fig. 3b evidences that peaks (1) and (2) are decreasing, peaks (3) and (4) are almost unchanged and peak (5) is increasing with increasing angle α as a result of the corresponding dipole transition vector components.

The analysis of the spectra for three fold coordinated O(3) in the second layer of the surface, see Figs. 2a, 5a and b, can be performed similar to that described above for O(1). The complex angle dependence is explained in close correspondence to that for the O(1) 1s excitations discussed above, using parallel and perpendicular components of the dipole transition vector, see Fig. 5b. The intensity of the lower energy part of the multi-peak structure consisting of peaks (1) and (2) seems to be increasing with increasing angle of incidence α. However, only the contribution of peak (2) increases, whereas peak (1) is vanishing with

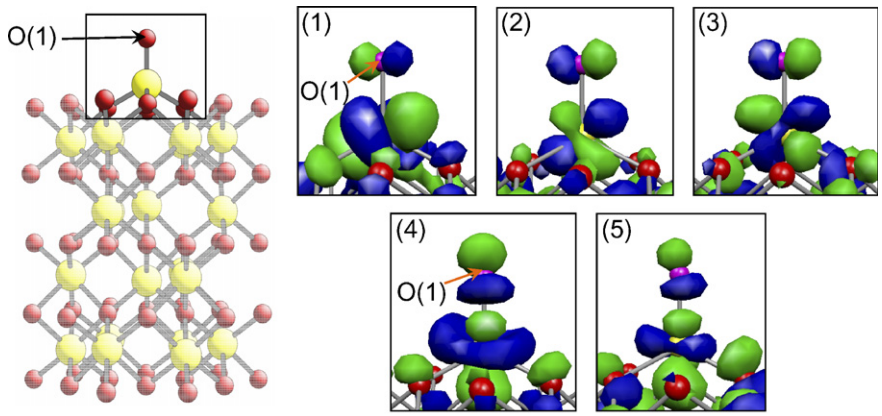

Fig. 4. Isosurface plots of selected final state orbitals for O(1) 1s core excitations corresponding to peaks 1–5 of Fig. 3a. Dark (blue) surfaces denote positive wavefunction values while light (green) surfaces refer to negative values. (For interpretation of the references to color in this figure, the reader is referred to the web version of this article.)

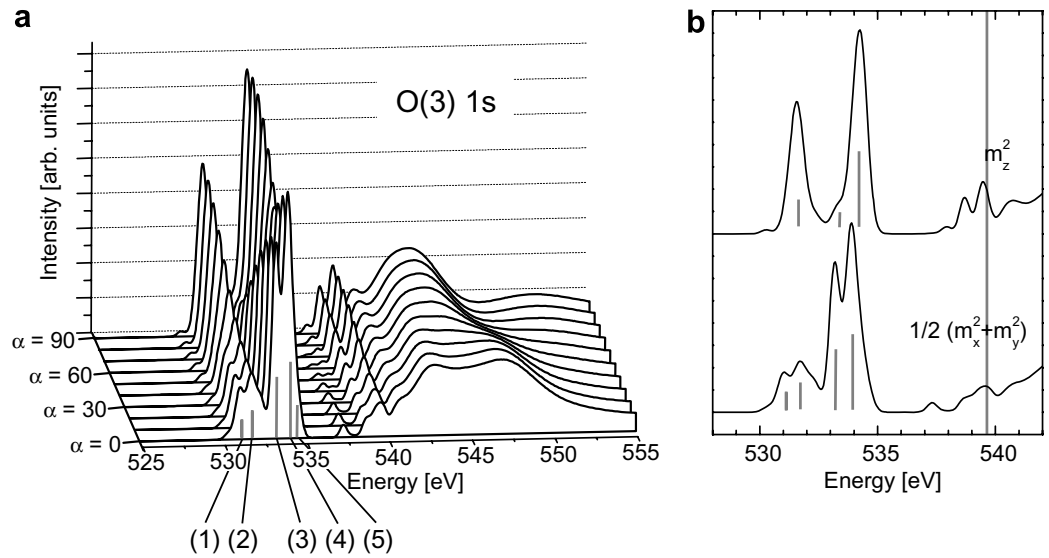

Fig. 5. Theoretical polarization-dependent NEXAFS spectra for the vanadyl terminated $V_2O_3(0001)$ surface. (a) Spectra of three fold coordinated oxygen, O(3), in the second surface layer. The angle of incidence of the photon beam α is given with respect to the surface normal. (b) Squared transition dipole matrix elements for O(3) 1s core excitations. The vertical gray line indicates the ionization threshold. Note that in both figures the energy scale has not been corrected for core hole relaxation and relativistic effects, see Section 2.

increasing α. This reflects the fact that the parallel component $m_{\|}$ dominates in peak (1) whereas the perpendicular component $m_{\perp}$ is the largest for peak (2), see Fig. 5b. The three peaks, (3)–(5), at higher energies are quite close in energy. Peak (3) at 533.2 eV and (4) at 534.0 eV are assigned to transitions into final state orbitals which are oriented parallel to the surface near the O(3) center. Hence the main component of the dipole transition vector is the parallel component $m_{\|}$ and the intensity of peaks (3) and (4) decreases with increasing incidence angle α. Peak (5) at 534.3 eV is due to final state orbitals consisting of p character perpendicular to the surface near the O(3) center and the dipole transition vector has a large perpendicular component $m_{\perp}$. Thus, the intensity of peak (5) increases with increasing incidence angle α, in contrast to that of peak (4). Since peaks (4) and (5) are very close in energy their superposition near 534 eV results in a rather weak variation with incidence angle α.

The oxygen centers of the third and fourth layer are both four fold coordinated while their interlayer distances differ. Centers in the fourth layer, $O(4)_{bulk}$, reflect the unperturbed bulk geometry, see Fig. 2a, whereas those of the third layer, $O(4)_{relaxed}$, are in a relaxed environment. Therefore, we have calculated NEXAFS spectra for both oxygen centers with the results shown in Fig. 6. As before, the spectra exhibit two energy regions, one above ionization threshold (about 540.4 eV for $O(4)_{relaxed}$ and about 540.6 eV for $O(4)_{bulk}$) and one below. The spectra of the third layer oxygen centers, $O(4)_{relaxed}$, see Fig. 6a, show a complex angle dependence in the energy region between

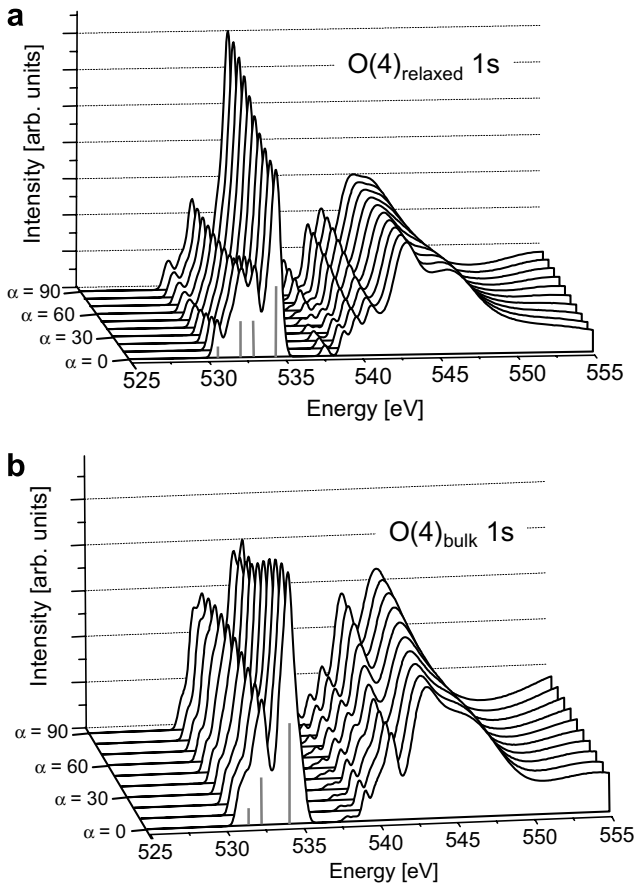

Fig. 6. Theoretical polarization-dependent NEXAFS spectra for the vanadyl terminated $V_2O_3(0001)$ surface. (a) Spectra of four fold coordinated oxygen, $O(4)_{relaxed}$, in the third surface layer. (b) Spectra of four fold coordinated oxygen, $O(4)_{bulk}$, in the fourth surface layer. The angle of incidence of the photon beam α is given with respect to the surface normal.

530 eV and 535 eV, which is explained, as before, by the geometric orientation of the final state orbitals with respect to the surface and the corresponding contributions to the dipole transition vector components. The spectra of the fourth layer centers, $O(4)_{bulk}$, see Fig. 6b, depend somewhat less on the angle of incidence α, which reflects the fact that the transition matrix elements for the two dipole directions $m_{\|}$ and $m_{\perp}$ are similar in size due to the quasi-tetrahedral geometry near the $O(4)_{bulk}$ centers.

Overall, the polarization-resolved NEXAFS spectra of the two four fold coordinated oxygen species are quite similar to each other while they show clear differences compared with the spectra of three fold coordinated O(3) and singly coordinated vanadyl oxygen O(1). Since, on the other hand, the O(3) and the O(1) derived spectra are quite different a discrimination between the different oxygen species based on the spectral features is possible. In particular, the dominant sharp peak in all O(1) 1s spectra, see Fig. 3a, which shows a weak angle dependence can be used as a fingerprint for singly coordinated vanadyl oxygen. The peak position shown in Fig. 3a at 532.5 eV needs to be corrected for electronic core hole relaxation and relativistic effects in order to allow a direct comparison with experiment. As discussed in Section 2 these corrections result in a global downwards shift of the theoretical energy scale by 1.4 eV resulting in 531.1 eV for the O(1) derived peak.

In Fig. 7 recent experimental polarization-resolved NEXAFS spectra are compared with theoretical spectra of vanadyl oxygen, O(1), core excitations for different incidence angles α of the photon beam (polar angles between the X-ray beam and the surface normal). The experimental spectra of Fig. 7a, full and dotted lines, reflect two differently prepared surfaces of $V_2O_3(0001)$. The first set (full lines) refers to a surface which was prepared according to the recipe of Section 3 and assigned to the vanadyl terminated surface based on additional experimental findings [24]. The second set (dotted lines) corresponds to the surface prepared as before but subsequently reduced by electron bombardment which removes most of the vanadyl groups as evidenced by STM [55], IRAS, and HREELS [24]. Thus, the difference spectra between the two sets, shown in Fig. 7b, can be assumed to yield the NEXAFS spectra of the surface vanadyl oxygen. In order to calculate these difference spectra the two initial data sets are normalized to yield the same height of the peak at 532.5 eV which, according to theory (uncorrected peaks near 534 eV in Figs. 5 and 6, see above and Section 2), consists mainly of contributions from bulk like oxygen, three- and four fold coordinated. We tried also other normalization schemes using peaks of both V 2p and O 1s core excitations which, however, result in only slightly different spectra.

Fig. 7c shows theoretical NEXAFS spectra referring to vanadyl oxygen, O(1), core excitations for incidence angles equal to those applied in the measurements. Here the theoretical energy scale has been shifted downwards by 1.4 eV (accounting for core hole relaxation and relativistic effects, see Section 2) in order to allow a direct comparison with experiment. The comparison of Figs. 7b and c evidences a prominent peak at 531.1 eV, both observed in the experiment and evaluated by theory, whose intensity is almost independent of the incidence angle α of the photon beam. Therefore, this peak can be taken as a clear fingerprint of singly coordinated vanadyl oxygen O(1). For small angles α a peak structure at lower energy, about 529 eV, is found in the experiment and confirmed by theory which is also assigned to excitations originating at vanadyl oxygen. However, its relative intensity appears to be smaller in theory than in experiment which remains unexplained so far. At the energy of 531.5 eV, i.e. above the fingerprint peak of vanadyl oxygen, a broad asymmetric peak is observed in the experiment. This peak is much narrower and visible in the theoretical spectra only for large angles α. This discrepancy may be explained by additional bulk oxygen contributions which are not completely removed in the experimental difference spectra. In addition, the spectra of the two terminations were measured at different beam lines with different experimental setups which may introduce further uncertainties. However, the overall agree-

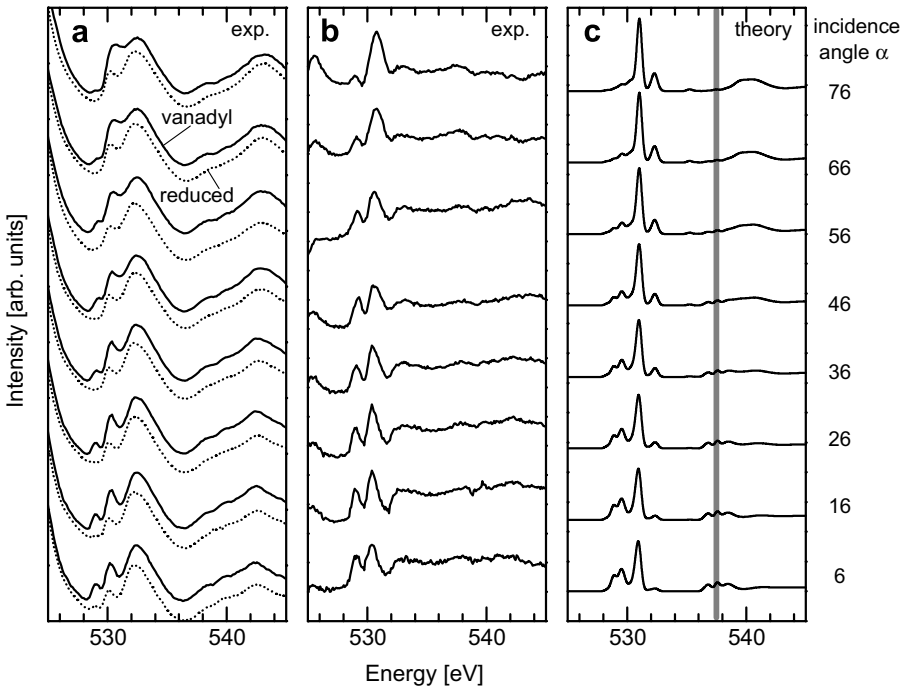

Fig. 7. Comparison of experimental and theoretical NEXAFS spectra for a set of different angles α of photon incidence, taken with respect to the surface normal: (a) experimental spectra normalized to peak at 532.5 eV. The straight (dotted) lines refer to the vanadyl terminated (reduced) surface. (b) Experimental difference spectra between the vanadyl terminated and reduced surface (spectra of (a)). (c) Theoretical NEXAFS spectra corresponding to core excitations of vanadyl oxygen, O(1). The vertical gray line in the theoretical NEXAFS spectra indicates the ionization threshold. For direct comparison with experiment the energy scale in (c) has been corrected for core hole relaxation and relativistic effects, see text.

ment between theory and experiment is very satisfactory confirming the theoretical approach.

5. Conclusions

The present ab initio DFT cluster studies on O 1s core excitations of the differently coordinated oxygen centers near the vanadyl terminated $V_2O_3(0001)$ surface can give a clear picture of the underlying electronic mechanisms. The resulting theoretical core excitation spectra are in good agreement with recent experimental polarization-dependent O 1s NEXAFS spectra for well ordered films of $V_2O_3(0001)$ on W(110) and Au(111) for which the vanadyl termination is suggested on experimental grounds [24]. With the present theoretical data the vanadyl surface termination is also proven on a theoretical basis.

The experimental spectra exhibit two main absorption regions which can be identified by the present theory as due to oxygen 1s core excitation involving differently coordinated oxygen species. First, the absorption region near 532 eV is characterized by O 1s core excitations to final state orbitals described as anti-bonding combinations of oxygen 2p and vanadium 3d contributions. Here the coordination of the corresponding oxygen species as well as its local binding geometry determines the polarization-dependent absorption. Second, the absorption region near 544 eV (above ionization threshold) can be assigned to electronic transitions from O 1s into final state orbitals with O 3p contributions where, as before, the local binding geometry determines the angle dependence of the spectra. A decomposition of the theoretical spectra into contributions of differently coordinated oxygen can give further insight into details of the experimental NEXAFS spectra. The corresponding oxygen species contribute differently to the spectra where, however, no obvious relation between the coordination number and energetic details of the transitions can be found. These results are in close analogy to former studies on the oxygen 1s NEXAFS spectra of V_2O_5 [50,51]. In order to be able to test other terminations of the $V_2O_3(0001)$ surface suggested by experiment under reducing conditions [24] or with different preparation methods [15] it would be interesting to study corresponding theoretical NEXAFS spectra in greater detail. Further, NEXAFS may be used to identify possible adsorption sites for molecules, such as methanol [56], at the $V_2O_3(0001)$ surface which is interesting from a catalytic point of view. Theoretical and experimental studies along these lines are currently under way.

Acknowledgements

This work was supported by Deutsche Forschungsgemeinschaft, Sonderforschungsbereich 546 "Transition Metal Oxide Aggregates". Prof. G. Kresse, University of Vienna, is kindly acknowledged for providing geometric information from his periodic slab calculations on vanadium sesquioxide surfaces [15].

References

[1] K. Hermann, M. Witko, in: D.P. Woodruff (Ed.), The Chemical Physics of Solid Surfaces (Oxide Surfaces), vol. 9, Elsevier Science, Amsterdam, 2001, p. 136.
[2] I.E. Wachs, Catal. Today 100 (2005) 79.
[3] G.C. Bond, S.F. Tahir, Appl. Catal. 71 (1991) 1.
[4] B. Grzybowska-Swierkosz, F. Trifiro, J.C. Vedrine (Eds.), Vanadia Catalysts for Selective Oxidation of Hydrocarbons and their derivatives, J. Appl. Catal. 157, 1997.
[5] G. Centi, S. Perathoner, F. Trifiro, Appl. Catal. A 157 (1997) 143.
[6] J.H. Choi, S.K. Kim, Y.C. Bak, Korean J. Chem. Eng. 18 (2001) 719.
[7] B.M. Weckhuysen, D.E. Keller, Catal. Today 78 (2003) 25.
[8] B. Tepper, B. Richter, A.C. Dupuis, H. Kuhlenbeck, C. Hucho, P. Schilbe, M.A. bin Yarmo, H.-J. Freund, Surf. Sci. 496 (2002) 64.
[9] R.L. Kurtz, V.E. Henrich, Phys. Rev. B 28 (1983) 6699.
[10] T. Uozumi, K. Okada, A. Kotani, R. Zimmermann, P. Steiner, S. Hufner, Y. Tezuka, S. Shin, J. Electr. Spectrosc. Relat. Phenom. 83 (1997) 9.
[11] S.Y. Ezhov, V.I. Anisimov, D.I. Khomskii, G.A. Sawatzky, Phys. Rev. Lett. 83 (1999) 4136.
[12] M. Catti, G. Sandrone, Faraday Discuss (1997) 189.
[13] E. Goering, M. Schramme, O. Muller, H. Paulin, M. Klemm, M.L. denBoer, S. Horn, Physica B 230 (1997) 996.
[14] G. Kresse, S. Surnev, M.G. Ramsey, F.P. Netzer, Surf. Sci. 492 (2001) 329.
[15] G. Kresse, S. Surnev, J. Schoiswohl, F.P. Netzer, Surf. Sci. 555 (2004) 118.
[16] V.E. Henrich, P.A. Cox, The Surface Science of Metal Oxides, University Press, Cambridge, 1994.
[17] M. Preisinger, J. Moosburger-Will, M. Klemm, S. Klimm, S. Horn, Phys. Rev. B 69 (2004).
[18] H. Niehus, R.P. Blum, D. Ahlbehrendt, Phys. Stat. Solidi A 187 (2001) 151.
[19] H. Niehus, R.P. Blum, D. Ahlbehrendt, Surf. Rev. Lett. 10 (2003) 353.
[20] J. Schoiswohl, M. Sock, S. Surnev, M.G. Ramsey, F.P. Netzer, G. Kresse, J.N. Andersen, Surf. Sci. 555 (2004) 101.
[21] J. Schoiswohl, M. Sock, S. Eck, S. Surnev, M.G. Ramsey, F.P. Netzer, G. Kresse, Phys. Rev. B 69 (2004) 155403.
[22] S. Surnev, G. Kresse, M. Sock, M.G. Ramsey, F.P. Netzer, Surf. Sci. 495 (2001) 91.
[23] S. Surnev, M.G. Ramsey, F.P. Netzer, Prog. Surf. Sci. 73 (2003) 117.
[24] A.C. Dupuis, M. Abu Haija, B. Richter, H. Kuhlenbeck, H.-J. Freund, Surf. Sci. 539 (2003) 99.
[25] I. Czekaj, K. Hermann, M. Witko, Surf. Sci. 525 (2003) 33.
[26] I. Czekaj, K. Hermann, M. Witko, Surf. Sci. 545 (2003) 85.
[27] T.K. Todorova, M.V. Ganduglia-Pirovano, J. Sauer, J. Phys. Chem. B 109 (2005) 23523.
[28] J. Schoiswohl, G. Tzvetkov, F. Pfuner, M.G. Ramsey, S. Surnev, F.P. Netzer, Phys. Chem. Chem. Phys. 8 (2006) 1614.
[29] G.S. Wong, M.R. Concepcion, J.M. Vohs, J. Phys. Chem. B 106 (2002) 6451.
[30] R.S. Weber, J. Phys. Chem. 98 (1994) 2999.
[31] O. Borck, E. Schroder, J. Phys. – Condens. Mat. 18 (2006) 10751.
[32] C. Kolczewski, K. Hermann, Theor. Chem. Acc. 114 (2005) 60.
[33] P.D. Dernier, M. Marezio, Phys. Rev. B 2 (1970) 3771.
[34] J.B. Goodenough, in: H. Reiss (Ed.), Prog. Solid State, 1971, p. 145 (Chapter 5).
[35] W.H. Zachariasen, Skrifter Norske Videnskaps – Akad. Oslo I. Mat.-Naturv. Klasse No. 4 (1928).
[36] R.W.G. Wyckoff, Crystal Structures, Interscience Publishers, New York, 1965.
[37] The program package StoBe is a modified version of the DFT-LCGTO program package DeMon, originally developed by A. St.-Amant and D. Salahub (University of Montreal), with extensions by K. Hermann and L.G.M. Pettersson.
[38] B. Hammer, L.B. Hansen, J.K. Nørskov, Phys. Rev. B 59 (1999) 7413.
[39] J.P. Perdew, K. Burke, M. Ernzerhof, Phys. Rev. Lett. 77 (1996) 3865.
[40] J.K. Labanowski, J.W. Anzelm (Eds.), Density Functional Methods in Chemistry, Springer-Verlag, New York 1991.
[41] N. Godbout, D.R. Salahub, J. Andzelm, E. Wimmer, Can. J. Chem. 70 (1992) 560.
[42] W. Kutzelnigg, U. Fleischer, M. Schindler, NMR-Basic Principles and Progress, Springer-Verlag, Heidelberg, 1990.
[43] L.G.M. Pettersson, U. Wahlgren, O. Gropen, J. Chem. Phys. 86 (1987) 2176.
[44] L.G.M. Pettersson, U. Wahlgren, O. Gropen, Chem. Phys. 80 (1983) 7.
[45] J.C. Slater, in: P.O. Loewdin (Ed.), Advances in Quantum Chemistry, vol. 6, Academic, New York, 1972, p. 1.
[46] J.C. Slater, K.H. Johnson, Phys. Rev. B 5 (1972) 844.
[47] H. Ågren, V. Carravetta, O. Vahtras, L.G.M. Pettersson, Theor. Chem. Acc. 97 (1997) 14.
[48] C. Kolczewski, R. Püttner, O. Plashkevych, H. Ågren, V. Staemmler, M. Martins, G. Snell, A.S. Schlachter, M. Sant'Anna, G. Kaindl, L.G.M. Pettersson, J. Chem. Phys. 115 (2001) 6426.
[49] L. Triguero, L.G.M. Pettersson, H. Ågren, Phys. Rev. B 58 (1998) 8097.
[50] C. Kolczewski, K. Hermann, J. Chem. Phys. 118 (2003) 7599.
[51] C. Kolczewski, K. Hermann, Surf. Sci. 552 (2004) 98.
[52] L. Triguero, O. Plashkevych, L.G.M. Pettersson, H. Ågren, J. Electr. Spectrosc. Relat. Phenom. 104 (1999) 195.
[53] O. Takahashi, L.G.M. Pettersson, J. Chem. Phys. 121 (2004) 10339.
[54] M. Abu Haija, S. Guimond, A. Uhl, H. Kuhlenbeck, H.-J. Freund, Surf. Sci. 600 (2006) 1040.
[55] S. Guimond, M. Abu Haija, S. Kaya, J. Lu, J. Weissenrieder, S. Shaikhutdinov, H. Kuhlenbeck, H.J. Freund, J. Döbler, J. Sauer, Top. Catal. 38 (2006) 117.
[56] M. Badlani, I.E. Wachs, Catal. Lett. 75 (2001) 137.